Scientific Reports

https://doi.org/10.1038/s41598-026-44950-2

Article in Press

Study on the hydraulic action mechanism and support measures of weakly cemented muddy surrounding rock

Received: 15 October 2025

Accepted: 16 March 2026

Published online: 04 April 2026

Cite this article as: Zaijiang Y., Weiguang Z., Zhijiang L. *et al.* Study on the hydraulic action mechanism and support measures of weakly cemented muddy surrounding rock. *Sci Rep* (2026). https://doi.org/10.1038/s41598-026-44950-2

Yu Zaijiang, Zhang Weiguang, Lun Zhijiang, Liu Shuaigang, Wang Rui, Wang Shuai & Zhao Leilei

Study on the Hydraulic action Mechanism and Support Measures of Weakly Cemented Muddy Surrounding Rock

Yu Zaijiang [a, b], Zhang Weiguang [a, b], Lun Zhijiang [a, b], Liu Shuaigang [c], Wang Rui [a, b], Wang Shuai [a, b], Zhao Leilei [a, b]

*(**a** Key Laboratory of Xinjiang Coal Resources Green Mining (Xinjiang Institute of Engineering), Ministry of Education, Urumqi 830023, China; **b** Xinjiang Engineering Research Center of Green Intelligent Coal Mining, Xinjiang Institute of Engineering, Urumqi 830023, China; **c** School of Resources & Environment Safety Engineering, Hunan University of Science and Technology, Xiangtan, 411201, China;)*

Abstract:

There are a large number of argillaceous weakly cemented strata distributed in western China, and their significant hydraulic characteristics seriously restrict the safe and efficient exploitation of coal resources. In order to solve the problem of deformation and failure of the surrounding rock roadway in this type of strata, this study systematically studied the hydraulic disintegration behavior of argillaceous weakly cemented rocks by comprehensively using laboratory tests, theoretical analysis, numerical simulation and field experiments, established a constitutive model of argillaceous weakly cemented rocks considering hydraulic effects, revealed the deformation and failure mechanism of this type of surrounding rock roadway, and developed the combined support technology of high-strength anchor rod-anchor cable. The technology was applied and verified in the No. 5 mine of Dananhu Lake. The results are as follows: (1) The dried

Funds: Xinjiang Tianshan Talent Training Program for Young Top-notch Talents (Research on the mechanism of disaster formation in weakly cemented roadway surrounding rock and the coordinated control technology of grouting modification-2024TSYCCX0051)
Key Research and Development Special Tasks of Xinjiang Province (No.2022B01051-3).
Opening Foundation of Key Laboratory of Xinjiang Coal Resources Green Mining (Xinjiang Institute of Engineering), Ministry of Education (KLXGY-KB2509).
Doctoral Startup Fund of Xinjiang Institute of Engineering (2025XGYBQJ56)
Xinjiang Uygur Autonomous Region Tianchi Elite Talent Innovation Leadership Program: 2024XGYTCYC03;
Urumqi City Hongshan Sci-Tech Innovation Elite Talents Youth Top Talents Program: B241013004;
National Key Research and Development Program Young Scientists Project: 2024YFC2910600;
Internal Project of Key Laboratory of Xinjiang Coal Resources GreenMining, Ministry of Education: KLXGY-Z2603;
About author: YU Zaijiang (1993-), male, from Shangqiu, Henan Province, Ph.D. Tel：15538905313， E-mail: yyzaijiang@126.com
Corresponding Author：ZHANG Weiguang (1986-), male, from Shangqiu, Henan Province, Ph.D. Tel：18129262579，E-mail: weiguang1228@126.com

argillaceous weakly cemented rock specimens are more prone to disintegration than those without drying treatment; (2) A mathematical model that can describe the mechanical behavior of argillaceous weakly cemented rocks under hydraulic action is constructed, and the effectiveness of the theoretical model is verified by triaxial compression test. (3) The stress distribution and deformation law of the surrounding rock of the roadway under different moisture content conditions were analyzed: with the increase of moisture content, the stress concentration area of the surrounding rock gradually shifted to the depth, and the extreme value of the principal stress difference increased significantly, resulting in the risk of deformation and instability of the roadway intensified, and the proximity of the top and bottom plate in the middle of the roadway also continued to increase. (4) The joint support parameters are determined by numerical simulation optimization: the diameter of the roof plate and the two anchors is 2400 mm, the length is 2400 mm, and the spacing is 800 × 800 mm; The anchor cable has a diameter of 18.9 mm, a length of 6300 mm, and a spacing of 2400 × 2400 mm. (5) The field test shows that the subsidence of the roadway roof, the amount of two gangs moving closer, the amount of bottom drum and the degree of roof damage are reduced by 35%, 26.1%, 50% and 35.7%, respectively. This study provides a theoretical basis and technical support for the stability control of argillaceous weakly cemented rock roadway.

Keywords: hydraulic action; weakly cemented muddy rock; high-strength bolt (cable) combined support; roadway support

Introduction

In recent years, the focus of coal mining in China has gradually shifted to Xinjiang. Due to the unique diagenetic environment, geological structures, and sedimentary processes, widely distributed weakly cemented muddy strata have formed in Xinjiang. Weakly cemented rock layers exhibit characteristics such as low strength, poor resistance to deformation, and weak stability in terms of mechanical properties. At the same time, this type of rock is significantly affected by hydro-physical processes; it tends to disintegrate when exposed to water, resulting in a sharp decrease in mechanical strength, low residual strength, and severe deformation under mining-induced stress.The significant weakening of the physical and mechanical properties of weakly cemented muddy surrounding rock when exposed to water leads to anchoring structure failure, severe roadway deformation, or even roof collapse, posing great challenges to the stability control of such roadways and seriously restricting the safe and efficient mining of coal resources in western China.[1-3].

Ji Hongguang and Song Chaoyang [4-15] systematically studied the physical and mechanical properties of weakly cemented sandstone in Hongqinghe Coal Mine in Inner Mongolia, deeply explored the correlation between its macroscopic mechanical behavior and mesoscopic structural

parameters, and constructed a macro-mesoscopic correlation model for the physical and mechanical properties of weakly cemented sandstone. In this study, the evolution process of the mesostructure of weakly cemented sandstone under water exposure conditions is reproduced by the PFC particle flow numerical simulation method, which provides an important theoretical basis for in-depth understanding of the mechanical behavior and permeability characteristics of this type of rock mass. Yao et al. [16] conducted compression tests on weakly cemented sandstone samples under different temperature and confining pressure conditions, and established a damage constitutive model that can consider the compaction stage and the residual deformation stage based on statistical damage theory. Yang Qi et al. [17] systematically analyzed the physical and mechanical properties of artificially frozen soft rock by conducting uniaxial compression and creep tests of soft rock at low temperature, and constructed a constitutive model suitable for the creep behavior of soft rock under low temperature conditions. Zhang, Jiabing et al. [18-20] studied the effects of freeze-thaw cycling on rock fatigue damage and stability, and clarified the long-term deformation behavior characteristics of rock masses in cold regions. Wang et al. [21] conducted loading tests on weakly cemented rock masses formed by hydrostatic osmotic rock mass, and the results showed that the secondary bearing capacity of this type of fractured rock mass increased significantly with the increase of rock particle size and strength.

Li Wei et al. [22] proposed a weakly cemented surrounding rock roadway support scheme using anchor mesh cable injection combined with steel frame. Wang Peng [23] proposed an optimization scheme for the control of the surrounding rock of the weakly cemented surrounding rock roadway according to the geological conditions of the specific mine. Wang et al. [24] proposed the use of secondary anchor net cable spray support to cope with the large deformation and failure of weakly cemented soft rocks. Zhang Weiguang and Zheng Xiaodong et al. [25] revealed through systematic research that the combined effect of tunneling disturbance and roof water spraying is the main factor inducing the roof disaster of weakly cemented roadway. He Guangliang et al. [26] systematically analyzed and compared the applicability of various sectional forms and support methods of weakly cemented soft rock roadways. Li Jun et al. [27] conducted an in-depth study on the deformation mechanism of weakly cemented surrounding rock inclined shafts. Gao Guangyuan [28] proposed the synergistic support technology of steel shed support and secondary mesh injection for the reinforcement of weakly cemented surrounding rock. Cai Jinlong [29] proposed a high-strength and high-preload coupling support structure to improve the stability of this type of surrounding rock.

n summary, existing research mainly focuses on the physical and mechanical behavior and characteristics of weakly cemented rock masses, their microstructural features, as well as post-peak strain softening and

dilation behavior. A relatively systematic understanding of the mechanical properties of argillaceous weakly cemented rock masses has been formed, and a series of targeted support measures have been proposed, achieving good results in practice. However, research on the strength degradation mechanism of argillaceous weakly cemented rock masses under hydromechanical effects and their constitutive models is still relatively weak, and the principles and methods for stability control of related surrounding rock roadways are not yet clear. This paper focuses on the deformation and failure issues of roadways in argillaceous weakly cemented surrounding rock, systematically studies the deformation characteristics of argillaceous weakly cemented rock under hydromechanical effects, establishes a constitutive relationship for argillaceous weakly cemented rock considering hydromechanical influence, conducts a reverse analysis of the deformation and failure process of surrounding rock roadways under hydromechanical effects, and proposes a combined deep and shallow hole grouting support technique, providing theoretical basis and technical support for the safe and efficient mining of coal seams in argillaceous weakly cemented surrounding rock.

1 Hydraulic Disintegration Test of Weakly Cemented Mudstone

Prepare clayey weakly cemented rock specimens with dimensions of 50× 50mm in diameter and height for a water absorption disintegration test. Place them in a container and add water until the specimens are completely submerged, then observe the disintegration behavior of the clayey weakly cemented rock under the action of water.

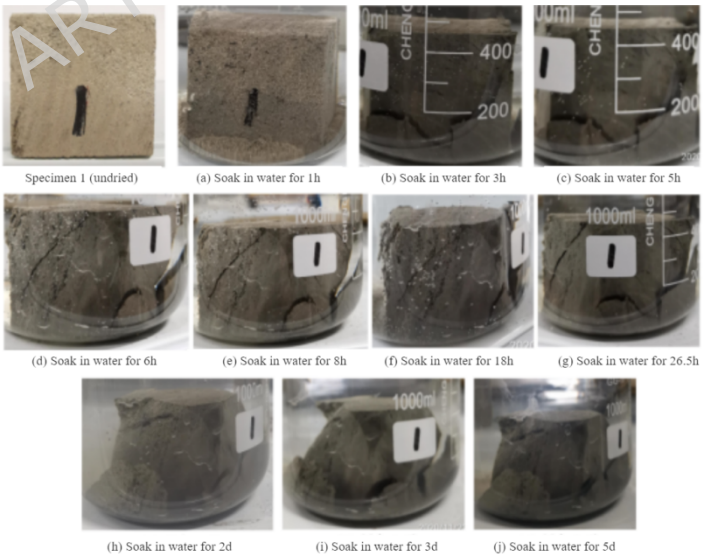

Figure 1 Weakly cemented rough rock meets water disintegration test

As shown in Fig.1, the clayey weakly cemented rock specimens that have not been dried start to absorb water and disintegrate after being soaked for 1 hour. Cracks gradually appear in the specimens in water, and the cracks

are well developed. The specimens gradually exhibit layer-by-layer peeling from the outside inward, and after peeling to a certain extent, the specimens disintegrate into relatively large blocks. With prolonged soaking, the large disintegrated blocks gradually break down into smaller pieces. The disintegration characteristics of the specimens are as follows:

1) The disintegration of muddy weakly cemented rock samples in water occurs relatively quickly. After 1.5 hours, the samples of muddy weakly cemented rock have mostly broken down from intact rock blocks into smaller fragments, accumulating at the bottom of the container.

2) After soaking in water, samples of weakly cemented muddy rock exhibit obvious disintegration into very small particles, causing the water in the container to become quite turbid.

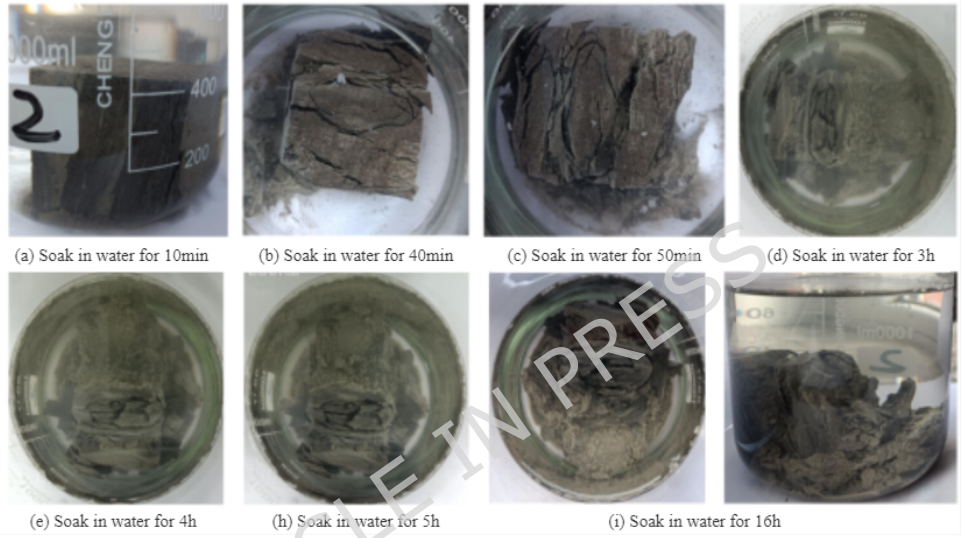

Figure 2 Water immersion test of weakly cemented surrounding rock after drying

As shown in Fig.2, after being soaked in water for 20 minutes in a container, the dried mudstone weakly cemented rock specimens exhibit softening and disintegration. During the softening and disintegration process, fractures develop well and are accompanied by the appearance of bubbles, making the water in the container turbid. The specimen gradually shows layer-by-layer peeling from the outside to the inside, and the peeled material gradually accumulates at the bottom of the container. After being soaked for 3 hours, the specimen disintegrates into relatively large blocks. With the extension of soaking time, the large disintegrated blocks gradually break into smaller ones. At this point, the specimen has completely lost its strength.

Due to the high content of expansive clay minerals in argillaceous weakly cemented rocks, as well as the presence of a large number of pores, water enters the pores when the rock is exposed to moisture and interacts with the expansive clay minerals, causing changes that lead to an increase in volume. Because argillaceous weakly cemented rocks exhibit anisotropic characteristics, the swelling forces generated at different locations vary, resulting in differing degrees of fracture development within the specimen,

which makes the internal structural differences more pronounced and ultimately leads to the disintegration of the specimen. Additionally, dried argillaceous weakly cemented rocks can undergo secondary water absorption, and both the water absorption rate and the disintegration rate of dried specimens are faster than those of undried specimens.

2 Construction of Numerical Models for Weakly Cemented Rocks Containing Cement

2.1 Analysis of the Failure Process of Cemented Weak Rocks

A typical stress-strain curve is obtained from a conventional triaxial compression test on samples of weakly cemented muddy rock, as shown in Fig.3, and is divided into four stages. The point of maximum compression at which volumetric strain corresponds to damage expansion stress is denoted as point A, which serves as the boundary. The elastic stage is the OA segment, the plastic stage (inelastic hardening yield segment) is the AB segment, the strain softening stage is the BC segment, and the residual stage is the CD segment. Based on the fundamental theory of elastoplastic mechanics, and fully considering the post-peak strain softening and dilatant deformation characteristics of weakly cemented muddy rock, a constitutive model of weakly cemented muddy rock is established based on hydraulic effects. This model reflects the strength and deformation characteristics of weakly cemented muddy rock under hydraulic influence and lays a foundation for revealing the deformation and failure mechanism of tunnels in weakly cemented muddy surrounding rock under hydraulic effects, thereby achieving stability control of tunnels in such surrounding rock.

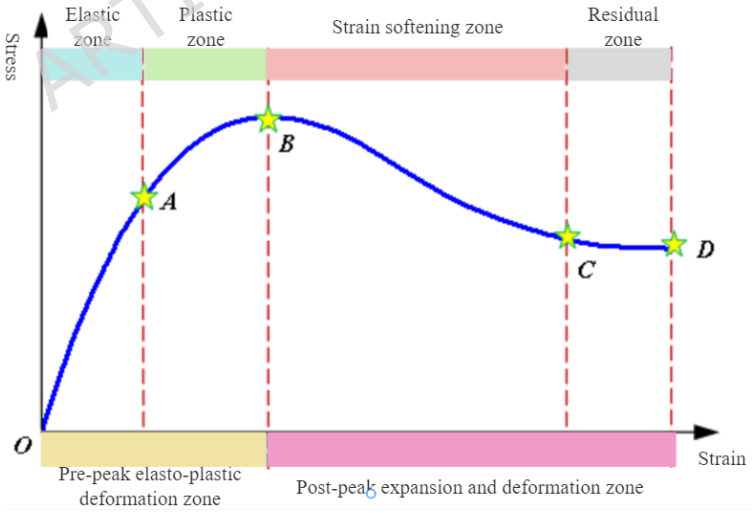

Figure 3 Schematic diagram of zoning division for stress-strain relationship of argillaceousweakly cemented rock

The total strain increment $d\varepsilon_{ij}$ includes the plastic strain increment $d\varepsilon_{ij}^{p}$ and the elastic strain increment $d\varepsilon_{ij}^{e}$, that is:

$$d\varepsilon_{ij} = d\varepsilon_{ij}^{e} + d\varepsilon_{ij}^{p} \quad (1)$$

The elastic strain increment $d\varepsilon_{ij}^{e}$ is obtained through the elastic increment theory, according to the generalized Hooke's law:

$$de_{ij}^{e} = C_{ijkl} ds_{kl} \quad (2)$$

In the formula, C_{ijkl} is the elastic compliance matrix;

$$C_{ijkl} = \frac{1}{E}\begin{bmatrix} 1 & -m & -m & 0 & 0 & 0 \\ -m & 1 & -m & 0 & 0 & 0 \\ -m & -m & 1 & 0 & 0 & 0 \\ 0 & 0 & 0 & 1+m & 0 & 0 \\ 0 & 0 & 0 & 0 & 1+m & 0 \\ 0 & 0 & 0 & 0 & 0 & 1+m \end{bmatrix} \quad (3)$$

Through the theory of plastic increments, determine the yield strength, clarify the loading and unloading conditions, understand the hardening-softening behavior, establish the plastic potential function, and ultimately obtain the required plastic strain increment.

2.2 Plastic potential function of the constitutive model

Plastic strain occurs during the loading process. The direction and magnitude of the plastic strain increment vector must be defined to describe the stress-strain relationship of elastoplastic deformation. The specification regarding the direction of the plastic strain increment is the flow rule of the plastic potential [30,31]. The direction of the plastic strain increment is orthogonal to the plastic potential surface and is along the normal to the plastic potential surface at that point:

$$d\varepsilon_{ij}^{p} = d\lambda \frac{\partial g(s_{ij}, k, w)}{\partial s_{ij}} \quad (4)$$

In the formula, g(σ_{ij},κ,w) is the plastic potential function; λ is the plastic flow factor.

The yield surface of geotechnical materials is not orthogonal to the plastic strain increment. When constructing the constitutive model, a non-associated plastic flow rule is adopted, and the plastic potential function is chosen as:

$$g(s_{ij}, k, w) = s_1 - K_y(k, w) s_3 \quad (5)$$

In the formula, K_ψ is related to the rock expansion characteristics, $K_\psi = (1+\sin\psi(\kappa, w))/(1-\sin\psi(\kappa, w))$; ψ is the expansion angle, which is related to κ and w.

2.3 Determination of the yield function in the constitutive model

The expression of the yield function in constitutive models considering stress, strain, and internal variables is:

$$f(s_{ij}, k, w) = 0 \quad (6)$$

In the formula, $f(\sigma_{ij},\kappa,w)$ is the yield function; κ is the hardening or softening parameter, determined according to the hardening or softening law of the yield surface.

When the yield function in the constitutive model follows the *Mohr-Coulomb* strength criterion, then:

$$f(s_{ij},k,w)=s_1-K_p(k,w)s_3-2c(k,w)\sqrt{K_p(k,w)}=0 \quad (7)$$

$$K_p(k,w)=\frac{1+\sin j(k,w)}{1-\sin j(k,w)} \quad (8)$$

In the formula, $c(\kappa,w)$ and $\varphi(\kappa,w)$ represent the cohesion and internal friction angle, respectively.

2.4 Determining the addition and removal conditions in the structural model

The current boundary of the elastic zone is determined by the yield surface in stress space. When the stress point is inside this surface, it is called an elastic state, exhibiting only elastic characteristics; when the stress state is on the yield surface, it shows a plastic state, possessing either elastic or plastic characteristics [32]. It is defined as follows:

$$\begin{cases} f<0, \text{ Elastic state} \\ f=0, \text{ Plastic state} \end{cases} \quad (9)$$

In the formula, f is the yield function, which is determined by the yield surface defined in the stress space.

The loading process occurs when the stress state of the hardened material develops beyond the yield surface, at which point elastoplastic deformation can be observed, causing additional plastic deformation. At the same time, to ensure that the stress state always remains on the subsequent loading surface, the current structure of the yield (or loading) surface also changes. During unloading, the stress state shows a tendency to exceed the yield point and continue moving inward, at which time elastic deformation occurs without changing the loading surface. Another possibility for stress change is that the stress point moves along the current yield surface; this phenomenon is called neutral deformation, which is accompanied by elastic deformation [33-35]. The criteria for neutral variable loading or unloading and loading are:

$f=0$ *and* $(\partial f/\partial\sigma_{ij})d\sigma_{ij}\leq 0$ corresponds to neutral loading or unloading, in which case we have:

$$de_{ij}=C_{ijkl}ds_{kl} \quad (10)$$

$f=0$ *and* $(\partial f/\partial\sigma_{ij})d\sigma_{ij}>0$ indicates loading, at which point we have:

$$de_{ij}=C_{ijkl}ds_{kl}+dl\frac{\partial g(s_{ij},k,w)}{\partial s_{ij}} \quad (11)$$

It can be seen from the plastic consistency condition:

$$\frac{\partial f}{\partial \sigma_{ij}} d\sigma_{ij} + \frac{\partial f}{\partial l} dl = 0 \quad (12)$$

Combining elastoplastic mechanical conditions:

$$d\sigma_{ij} = D_{ijkl} \varepsilon_{kl}^{e} = D_{ijkl} \left(\varepsilon_{kl} - \varepsilon_{kl}^{p} \right) \quad (13)$$

In the formula, D_{ijkl} is the elastic stiffness matrix, $D_{ijkl}=C_{ijkl}^{1}$.

By combining the above equations, the plastic flow factor can be determined as:

$$dl = \frac{\frac{\partial f}{\partial \sigma_{ij}} d\sigma_{ij}}{-\frac{\partial f}{\partial k} \frac{\partial k}{\partial \varepsilon_{ij}^{p}} \frac{\partial g}{\partial \sigma_{ij}} + \frac{\partial f}{\partial \sigma_{ij}} C_{ijkl} \frac{\partial g}{\partial \sigma_{kl}}} \quad (14)$$

2.5 The hardening-softening law is determined in the constitutive model

The stress within a rock acting on a certain yield surface can generate new elastic and plastic strains under external loads, forming new yield surfaces and causing changes in the stress on the original yield surfaces. When the stress variation remains within the range enclosed by the yield surface, only elastic strain occurs, which does not alter the state of the original yield surface [36-39]. The expansion, movement, or alteration of the form of a yield surface can be achieved through loading. The material's stress path and magnitude determine the extent, position, and form of these changes, which are referred to as hardening (or softening), as shown in Fig.4.

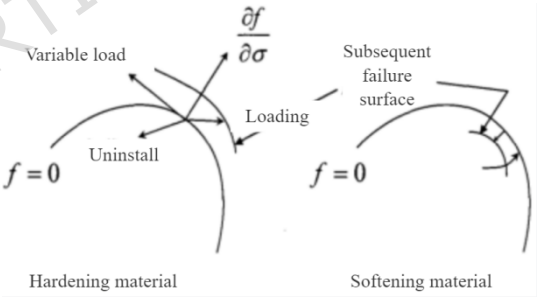

Figure4 Schematic diagram of hardening or softening of rock mass material

The magnitude of plastic strain and the changes in the yield surface are determined by the hardening law, usually expressed as a function containing κ. There are two ways to determine the value of κ :

（1）κ is characterized as a function of plastic strain, such as plastic shear strain γp, expressed as:

$$\gamma^{p} = \left| \varepsilon_{1}^{p} - \varepsilon_{3}^{p} \right| \quad (15)$$

（2）κ is characterized as a function of the plastic strain increment, such as the equivalent plastic strain $\bar{\varepsilon}^{p}$, and is expressed as:

$$\bar{e}^{p} = \sqrt{2\left(de_1^{p}de_1^{p} + de_2^{p}de_2^{p} + de_3^{p}de_3^{p}\right)/3} \quad (16)$$

In numerical software such as UDEC and FLAC, its equivalent plastic strain expression e^{ps} is:

$$e^{ps} = \sqrt{\frac{\left(De_1^{ps} - De_m^{ps}\right)^2 + \left(De_m^{ps}\right)^2 + \left(De_3^{ps} - De_m^{ps}\right)^2}{2}} \quad (17)$$

In the formula, De_1^{ps}、De_3^{ps} is the plastic shear major strain increment; De_m^{ps} is the mean of plastic shear principal strain increments, $De_m^{ps} = \left(De_1^{ps} + De_3^{ps}\right)/3$.

2.6 Mapping Relationship between Strength Parameters of Weakly Cemented Mudrock and Plastic Parameters of Strain Softening Model

In the UDEC simulation software, the equivalent plastic strain e^{ps} is used as the hardening-softening parameter. To establish the mapping relationship between post-peak strength parameters and plastic parameters, the evolution laws of cohesion, internal friction angle, and dilation angle of muddy weakly cemented rock with respect to the plastic parameters are considered, and their mapping relationship is simplified into a piecewise linear function.

The relationship between the strength parameters and the dilation angle with the equivalent plastic strain in clayey weakly cemented rocks is as follows.:

$$c = \begin{cases} c_0 & e^{ps} \le e_{co}^{ps} \\ c_0 - \dfrac{c_0 - c_r}{e_{cr}^{ps}} e^{ps} & e_{co}^{ps} \le e^{ps} \le e_{cr}^{ps} \\ c_r & e^{ps} \ge e_{cr}^{ps} \end{cases} \quad (18)$$

$$j = \begin{cases} j_0 & e^{ps} \le e_{jo}^{ps} \\ j_0 + \dfrac{j_r - j_0}{e_{jr}^{ps}} e^{ps} & e_{jo}^{ps} \le e^{ps} \le e_{jr}^{ps} \\ j_r & e^{ps} \ge e_{jr}^{ps} \end{cases} \quad (19)$$

$$y = \begin{cases} y_0 & e^{ps} \le e_{yo}^{ps} \\ y_0 - \dfrac{y_0 - y_r}{e_{yr}^{ps}} e^{ps} & e_{yo}^{ps} \le e^{ps} \le e_{yr}^{ps} \\ y_r & e^{ps} \ge e_{yr}^{ps} \end{cases} \quad (20)$$

In the formula, c_0、φ_0、ψ_0 refers to the damage expansion stress (corresponding respectively to cohesion, internal friction angle, and dilation angle; c_r、φ_r、ψ_r are the corresponding residual stresses; ε_{co}^{ps}、ε_{cr}^{ps}、$\varepsilon_{\varphi o}^{ps}$、$\varepsilon_{\varphi r}^{ps}$、$\varepsilon_{\psi o}^{ps}$、$\varepsilon_{\psi r}^{ps}$ are the corresponding critical plastic strain parameter.

2.7 Verification of Mathematical Model of Muddy Weakly Cemented Rock under Hydraulic Action

In order to verify whether the corrected microscopic mechanical parameters are reasonable, the aforementioned rock mass parameters need to be applied to the triaxial compression model, and the simulation results should be compared with laboratory data. During the numerical simulation, the specimen dimensions are set to a width of 2 meters and a height of 4 meters. The specific experimental results are shown in Fig.5.

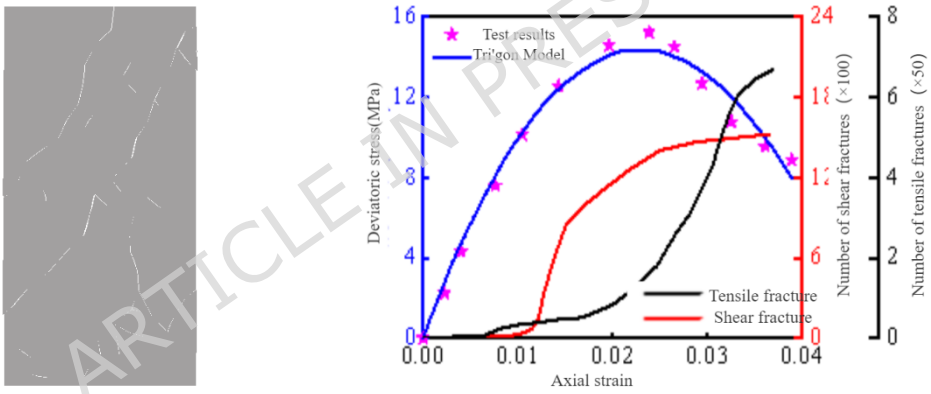

(a)Destructive form　　(b)Triaxial Compression Simulation Test

Figure 5 Stress-strain curve of simulated testing on argillaceous weakly cemented rock mass under water-rock interaction

As shown in Fig.5, under triaxial compression conditions, tensile cracks initially appear in the muddy weakly cemented rock mass when the load reaches 31% of the peak stress; as the load increases to 54% of the peak stress, shear cracks begin to appear; when the load reaches 79% of the peak stress, the number of shear cracks increases rapidly. The simulation results indicate that the peak stress and elastic modulus of the muddy weakly cemented rock mass are 15 MPa and 1.84 GPa, respectively, which are basically consistent with laboratory results. Therefore, the revised joint parameters of the muddy weakly cemented rock mass and its bulk constitutive model are highly reasonable.

3 Deformation and failure process of tunnels in weakly cemented surrounding rock containing cement

3.1 Construction of UDEC-Trigon Modified Model for Deformation and Failure Process of Weakly Cemented Surrounding Rock Tunnel

A two-dimensional UDEC model was established to simulate the deformation and failure process of weakly cemented muddy surrounding rock tunnels under hydrological effects. The numerical model is shown in Fig.6. The model has a width of 240 m and a height of 80 m. To improve computational efficiency, the study area was discretized using the UDEC Trigon model for joint blocks. The average size of triangular blocks within the study area is 0.2 m. Coarser polygonal Trigon blocks with an average size of 0.5 m were used to simulate the coal seam, and coarser polygonal Trigon blocks with average sizes of 1.0 m and 2.0 m were used to simulate the coal-bearing strata at the model boundaries. The bottom and side boundaries of the model are fixed in vertical and horizontal directions, respectively, and a vertical stress of 5.5 MPa, equivalent to the weight of a 220 m overlying rock layer, is applied to the upper boundary of the model, with a horizontal-to-vertical stress ratio of 1.2.

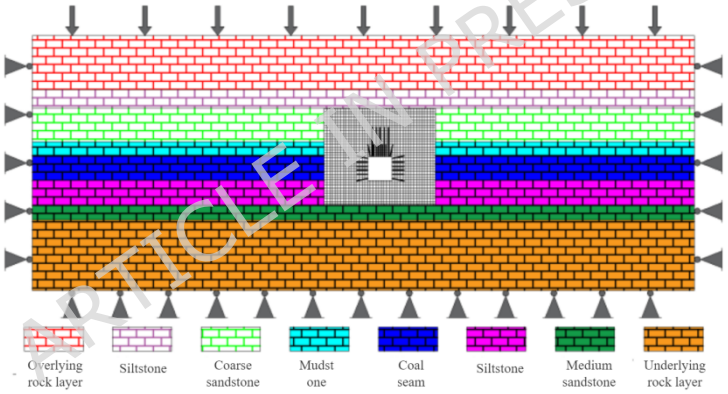

Figure 6 UDEC Trigon model for simulating deformation and failure of the roadway in argillaceous weakly cemented surrounding rock

3.2 Evolution Pattern of Stress Field in Weakly Cemented Mudstone Tunnel Surrounding Rock

The moisture content of weakly cemented muddy surrounding rock has a significant impact on the distribution of vertical stress in roadway surrounding rock. The evolution pattern of the vertical stress distribution cloud map of weakly cemented muddy roadway surrounding rock under hydraulic action is shown in Fig.7. A measurement line is taken from the middle of the roadway roof towards the interior of the roadway to obtain the vertical stress distribution of the roadway roof and both sides of the surrounding rock of weakly cemented muddy roadway under hydraulic action, as shown in Fig.8.

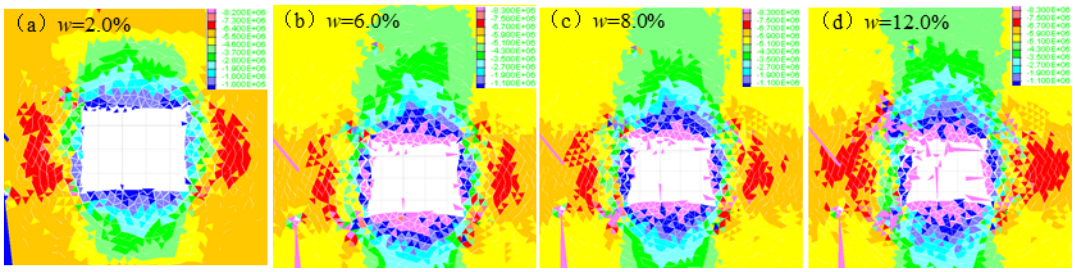

Figure 7 Evolution pattern of vertical stress contour in the surrounding rock of the argillaceous weakly cemented roadway under water-rock interaction

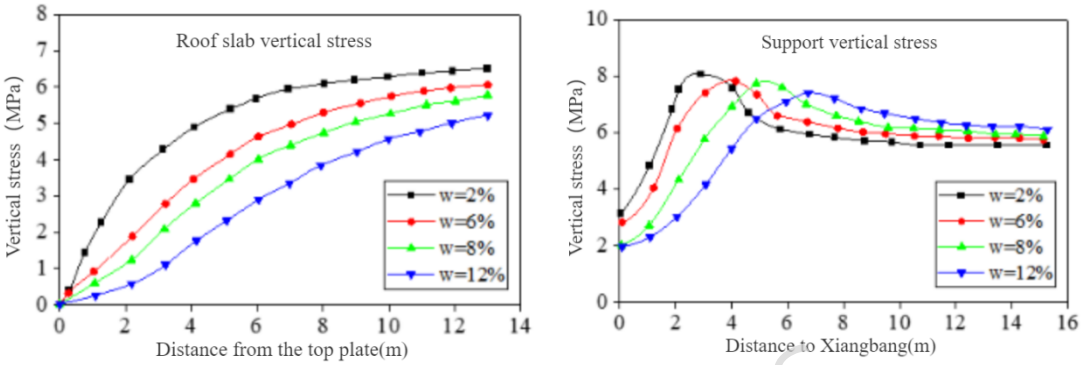

（a）Vertical stress on the roadway roof （b）Ore Drift Support Vertical Stress

Figure 8 Variation pattern of vertical stress distribution curve in the rock mass surrounding an argillaceous weakly cemented roadway subject to water-rock interaction

Combining Fig.7 and 8, it can be seen that: under different water content conditions, the vertical stress distribution in the mudstone weakly cemented roadway surrounding rock is basically the same. From the roadway surface to the deep surrounding rock, there are sequentially a stress reduction zone, a stress increase zone, and an original rock stress zone; water content has a significant impact on the evolution characteristics of the vertical stress in the mudstone weakly cemented surrounding rock. As the water content increases, the position of stress concentration in the mudstone weakly cemented roadway surrounding rock gradually moves away from the roadway surface, increasing from 3.1 m from the roadway rib at a water content of 2% to 6.7 m at a water content of 6%. With the increase in water content, the peak values of vertical stress at both ribs of the mudstone weakly cemented roadway slightly decrease.

The failure of the surrounding rock is related to the shear modulus, and the principal stress difference s_m is equal to the maximum principal stress minus the minimum principal stress.

$$s_m = |s_1 - s_2| \quad (21)$$

In the formula: s_1 is maximum principal stress; s_2 is minimum principal stress.

The water content in weakly cemented argillaceous surrounding rock significantly affects the distribution of principal stress differences within the tunnel surrounding rock. Under hydraulic action, the evolution pattern of the principal stress difference distribution cloud map in weakly cemented argillaceous tunnel surrounding rock is shown in Fig.9. By selecting a measurement line from the central part of the tunnel roof towards the interior of the tunnel, the principal stress difference distribution in weakly cemented argillaceous tunnel surrounding rock under hydraulic action is obtained, as shown in Fig.10.

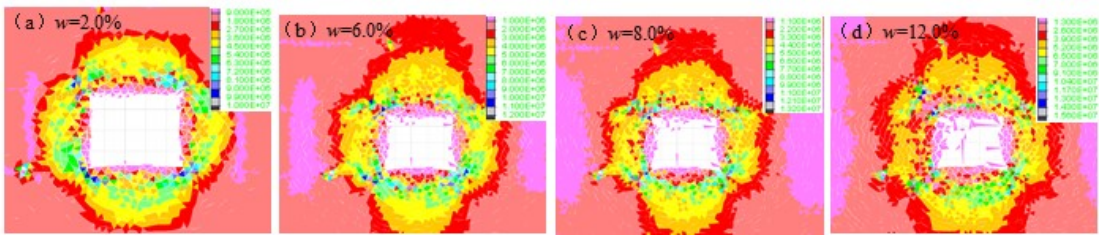

Figure 9 Evolution pattern of the major stress difference contour in the surrounding rock of the argillaceous weakly cemented roadway under water-rock interaction

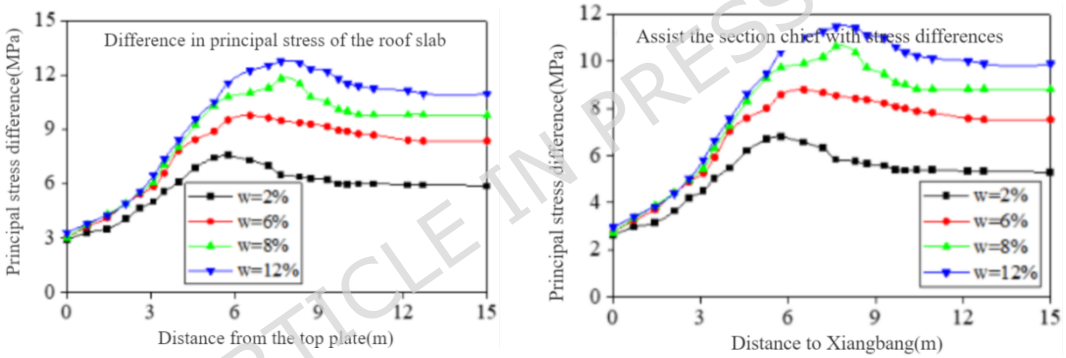

(a) The main stress of the roadway roo is poor

(b) The main stress in the roadway support is uneven.

Figure 10 Variation pattern of the major stress difference distribution curve in the rock mass surrounding an argillaceous weakly cemented roadway subject to water-rock interaction

Combining Fig.9 and 10, it can be seen that: moisture content has a significant effect on the differential stress distribution of argillaceous weakly-cemented surrounding rock, although the differential stress cloud maps of argillaceous weakly-cemented surrounding rock with different moisture contents are similar. As the depth of the surrounding rock increases, the differential stress of the roadway roof initially increases and then decreases, eventually stabilizing. For argillaceous weakly-cemented surrounding rock with different moisture contents, the differential stress curves are similar in shape, but the extreme values increase with higher moisture content. When the moisture content reaches 12%, the peak differential stress of the roof and the sidewalls reaches approximately 13.0 MPa and 11.8 MPa, respectively, with the roof peak occurring at about 6.0 m

depth and the sidewall peak at approximately 5.0 m. In addition, both the maximum differential stress and the displacement at the edge of the roadway increase with moisture content, reaching a maximum displacement of 7.6 m at 12% moisture content. Therefore, within the moisture content range of 8–12%, not only do the extreme values of differential stress significantly increase, but their peak positions are also farther from the roadway surface. This indicates that moisture content has a significant impact on the stress distribution of argillaceous weakly-cemented surrounding rock, and its increase can exacerbate roadway deformation and instability risks.

3.3 Deformation Evolution Law of Tunnels in Weakly Cemented Mudstone Surrounding Rock

After the excavation of the roadway, the mudstone weakly cemented surrounding rock changes from a triaxial stress state to a biaxial stress state, and the surrounding rock of the roadway is squeezed into the free space at the excavation. After the roadway excavation, the mudstone weakly cemented roof rock layer tends to move downward. With the continuous action of stress, phenomena such as roof subsidence, inward contraction of the two sides, and floor heaving occur in the surrounding rock of the roadway. The deformation pattern of the mudstone weakly cemented surrounding rock under hydrogeological action is shown in Fig.11. Monitoring points are arranged at the two sides, roof, and floor of the roadway. By monitoring the displacement changes on the surface of the surrounding rock after roadway excavation, the monitoring results are shown in Fig.12.

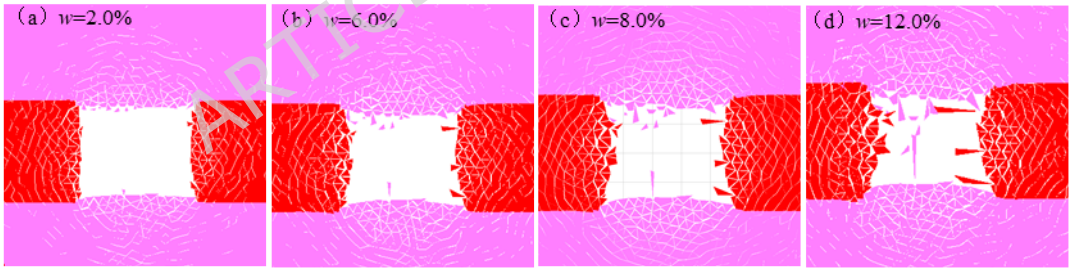

Figure 11 Variation pattern of deformation characteristics in the roadway with argillaceous weakly cemented surrounding rock under water-rock interaction

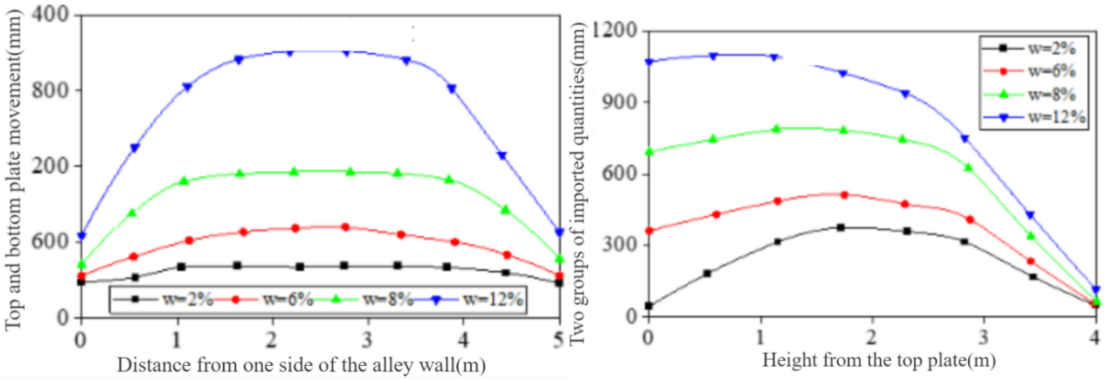

(a) Amount of roadway roof and floor convergence

(b) The amount of shift of the two sides of the alley

Figure12 Variation pattern of deformation magnitude in the roadway with argillaceous weakly cemented surrounding rock under water-rock interaction

As can be seen from Fig.11 and 12: with the increase of water content, the convergence of the roof and floor gradually increases, and the rate of increase gradually grows. In the roadway with muddy weakly cemented surrounding rock, the convergence of the roof and floor in the middle section of the roadway increases from 410 mm at a water content of 2% to 2110 mm at a water content of 12%. With the increase of water content, under the influence of roof subsidence, the convergence of the two sidewalls in the middle section of the roadway increases from 374 mm at a water content of 2% to 1020 mm at a water content of 12%.

4 Combined Control Technology of Anchor Bolts (Anchor Cables) and On-Site Application

4.1 Principle of Active Support Using High-Strength Anchor Bolts (Anchor Cables)

Rock bolts (or anchor cables) improve the overall bearing performance of the surrounding rock through anchoring and form an anchorage-bearing layer in weak argillaceous cemented surrounding rock, as shown in Fig.13. Weak argillaceous cemented surrounding rock contains numerous fractures, bedding planes, joints, and other geological weak planes. Under external loads, these weak planes may open or slip, causing deformation of the surrounding rock in tunnels. Rock bolts (or anchor cables) apply radial anchoring forces to the surrounding rock, effectively transforming the shallow surrounding rock from a plane stress state to a more stable triaxial stress state, thereby significantly enhancing the stability of the shallow surrounding rock. Additionally, rock bolts (or anchor cables) apply tangential anchoring forces to improve the mechanical properties of the surrounding rock structures, ensuring that local weak zone failure does not lead to overall instability, thereby increasing the load-bearing capacity and overall stability of the surrounding rock.

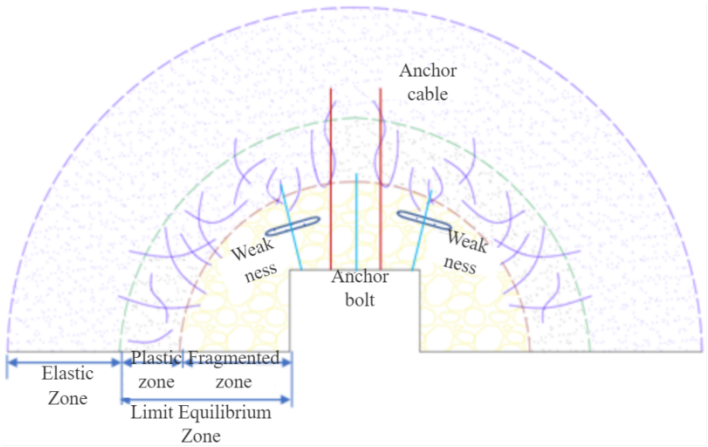

Figure 13 Anchoring and bearing structure reinforced by high-strength rock bolts and anchor cables for the surrounding rock of weakly cemented muddy roadway

4.2 Determination of Anchor Bolt (Anchor Cable) Support Parameters

Based on the production geological conditions of the No. 5 DaNanHu Mine, and according to the principles of bolt (anchor cable) support, the spacing of bolts in the return airway of the 1801 working face in weak clayey surrounding rock is determined to be 700mm~1000mm. The bolt length is set to 2000mm~2600mm, the anchor cable length to 4300mm~8300mm, and the anchor cable diameter to 17.8mm~21.6mm. The comparative scheme of the parameters is shown in Tab.1.

Table 1 Comparison scheme of bolt (cable) parameters

Serial Number	Parameter	Range of values（mm）
1	Anchor rod length	2000、2200、2400、2600
3	Spacing between anchor rods	700、800、900
4	Anchor cable length	4300、6300、8300
5	Anchor cable diameter	17.8、18.9、21.8

（1）Length of top anchor bolt

To obtain the appropriate length for the primary roof anchor, specific parameter conditions were set during the numerical simulation: both the primary and secondary roof anchors were assigned a diameter of 22mm, with the secondary roof anchor fixed at a length of 2400mm, and the spacing between them uniformly set at 800mm; the anchor cable was assigned a diameter of 21.8mm and a length of 6300mm, with a spacing of 2400mm between cables. By adjusting the length of the primary roof anchor, the deformation pattern of tunnels in weak clayey and poorly cemented surrounding rock was simulated and analyzed, with the related simulation results shown in Fig.14.

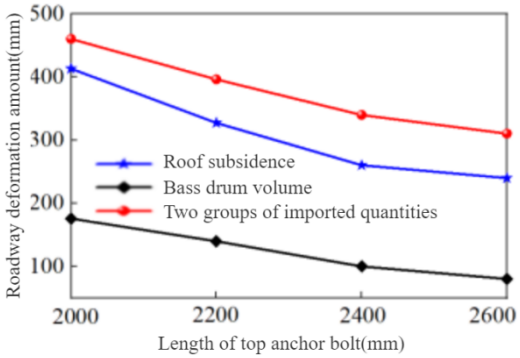

Figure 14 Effect of the length of rock bolt in roof on the deformation of the argillaceous weakly cemented surrounding rock roadway

As shown in Fig.14, the length of the top anchor bolt has a significant impact on the deformation of roadways in weakly cemented mudstone

surrounding rock. When the top anchor bolt length increases from 2000 mm to 2400 mm, the roof subsidence of the weakly cemented mudstone roadway decreases by 37.0%, the convergence of the two sides decreases by 26.1%, and the floor heave decreases by 43.1%. As the top anchor bolt length further increases from 2400 mm to 2600 mm, the deformation of the weakly cemented mudstone roadway does not show significant change, indicating that the suitable top anchor bolt length is 2400 mm.

（2）Assist with anchor bolt length

To obtain the appropriate length for the auxiliary anchor rod, specific parameter conditions were set during the numerical simulation: both the top anchor rod and the auxiliary anchor rod were chosen to have a diameter of 22 mm, with the length of the top anchor rod fixed at 2400 mm, and the spacing between them uniformly set at 800 mm; the anchor cable was set with a diameter of 21.8 mm and a length of 6300 mm, with a spacing of 2400 mm. By adjusting the length of the auxiliary anchor rod, a simulation analysis of the deformation pattern of the weakly cemented muddy surrounding rock roadway was conducted. The related simulation results are shown in Fig.15.

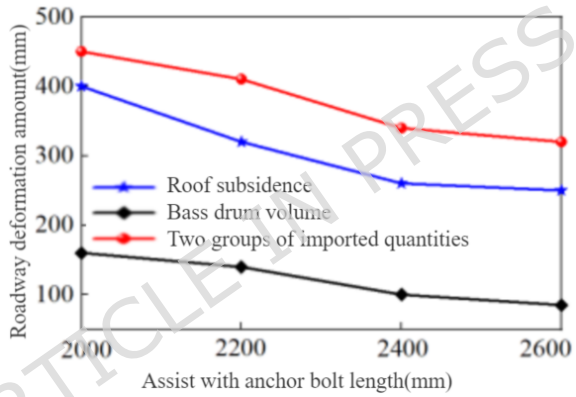

Figure 15 Effect of the length of the rock bolts in rib on the deformation of the argillaceous weakly cemented surrounding rock roadway

As shown in Fig.15, the length of the auxiliary anchor bolts has a significant impact on the deformation of roadways in weak argillaceous cemented surrounding rock. When the auxiliary anchor bolt length increases from 2000 mm to 2400 mm, the roof subsidence of the roadway in weak argillaceous cemented surrounding rock decreases by 35.0%, the convergence between both sides decreases by 24.4%, and the floor heave decreases by 37.5%. However, when the auxiliary anchor bolt length increases from 2400 mm to 2600 mm, there is no significant change in the deformation of the roadway, indicating that the appropriate length of the auxiliary anchor bolts is 2400 mm.

（3）Spacing between anchor rods

In order to obtain an appropriate spacing for the rock bolts, specific parameter conditions were set during the numerical simulation: the diameters of both the top bolt and the side bolt were chosen to be 22 mm, with their lengths fixed at 2400 mm; the diameter of the anchor cable was

set to 21.8 mm, and its length was set to 6300 mm, with a spacing of 2400 mm between the cables. By adjusting the spacing of the rock bolts, the deformation patterns of tunnels in muddy weakly cemented surrounding rock were simulated and analyzed. The relevant simulation results are shown in Fig.16.

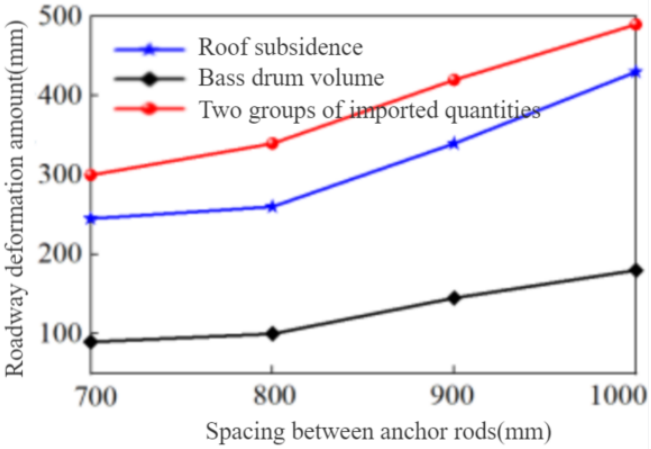

Figure 16 Effect of the row spacing between rock bolts on the deformation of the argillaceous weakly cemented surrounding rock roadway

As shown in Fig.16, the spacing between anchor bolts significantly affects the deformation of tunnels in mudstone weakly cemented surrounding rock. When the spacing between anchor bolts is reduced from 1000 mm to 800 mm, the roof subsidence of the tunnel in mudstone weakly cemented surrounding rock decreases by 39.5%, the convergence of the two sides decreases by 30.6%, and the floor heave decreases by 44.4%. However, when the spacing is further reduced from 800 mm to 700 mm, the deformation of the tunnel does not show significant changes. Therefore, the appropriate spacing between anchor bolts is 800 mm.

（4）Determination of anchor cable length

In order to obtain the appropriate anchor cable length, specific parameter conditions were set during the numerical simulation process: the diameters of the primary and auxiliary anchor rods were both selected as 22mm, with the lengths of the primary and auxiliary anchor rods fixed at 2400mm, and the spacing between them uniformly set at 800mm; the diameter of the anchor cable was set at 21.8mm, with a uniform spacing of 2400mm between anchor cables. By adjusting the length of the anchor cables, the deformation pattern of tunnels in weakly cemented muddy surrounding rock was simulated and analyzed, and the related simulation results are shown in Figure 17.

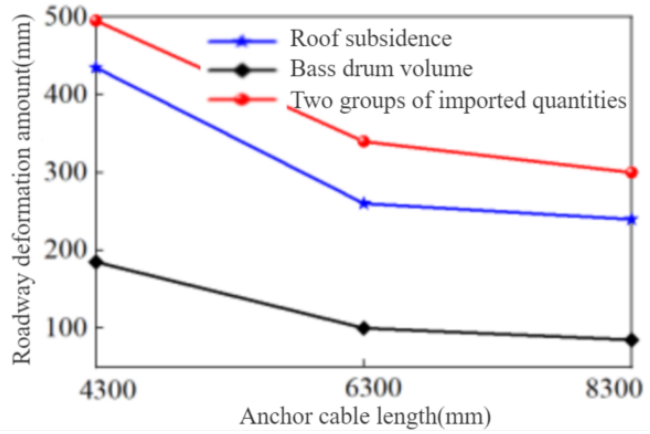

Figure 17 Effect of anchor cable length on the deformation of argillaceous weakly cemented surrounding rock roadway

As shown in Fig.17, the length of the anchor cable has a significant impact on the deformation of tunnels in weakly cemented muddy surrounding rock. When the anchor length increases from 4300 mm to 6300 mm, the roof subsidence of tunnels in weakly cemented muddy surrounding rock decreases by 40.0%, the convergence between the two sides decreases by 31.3%, and the floor heave decreases by 45.9%. When the anchor length increases from 6300 mm to 8300 mm, the roof subsidence decreases by 7.7%, the convergence between the two sides decreases by 13.2%, and the floor heave decreases by 15.0%, showing only minor changes in tunnel deformation. Considering the roof strata conditions of the return air roadway in the 1801 working face of the Dananhu No. 5 Mine, an appropriate anchor length is determined to be 6300 mm.

（5）Determination of anchor cable diameter

In order to obtain the appropriate anchor cable diameter, specific parameter conditions were set during the numerical simulation process: the diameters of the primary and auxiliary anchor rods were both selected as 22mm, with the lengths of the primary and auxiliary anchor rods fixed at 2400mm, and the spacing between them uniformly set at 800mm; the length of the anchor cable was set at 6300mm, with the spacing between anchor cables set at 2400mm. By adjusting the diameter of the anchor cable, the deformation pattern of roadways in mudstone weakly-cemented surrounding rock was analyzed through simulation, and the related simulation results are shown in Fig.18.

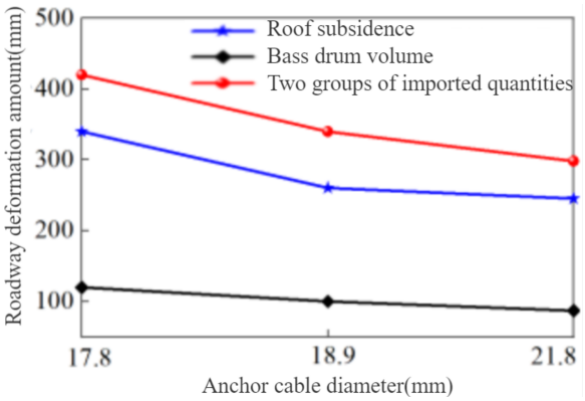

Figure 18 Effect of anchor cable diameter on the deformation of argillaceous weakly cemented surrounding rock roadway

As shown in Fig.18, the diameter of anchor cables has little effect on the deformation of tunnels in weak argillaceous cemented surrounding rock. When the anchor diameter increases from 17.8 mm to 18.9 mm, the roof subsidence of the tunnel in weak argillaceous cemented surrounding rock decreases by 23.5%, the convergence of the two sides decreases by 19.0%, and the floor heave decreases by 16.7%. When the anchor diameter increases from 18.9 mm to 21.8 mm, the roof subsidence decreases by 5.8%, the convergence decreases by 12.4%, and the floor heave decreases by 5.0%, indicating that the variation in tunnel deformation is minor. Therefore, the suitable anchor diameter is 18.9 mm.

In summary, through numerical simulation, the influence of changes in bolt (anchor cable) support parameters on the deformation of mudstone weakly cemented surrounding rock in tunnels was analyzed, and the bolt (anchor cable) support parameters for the 1801 return airway of the Dananhu No. 5 Mine were determined: roof and sidewall bolts with a diameter of 22 mm and a length of 2400 mm, arranged at a spacing of 800×800 mm; anchor cables with a diameter of 18.9 mm and a length of 6300 mm, arranged at a spacing of 2400×2400 mm.

4.3 On-site testing

To improve the stability of roadways in mudstone weakly cemented surrounding rock, drainage holes are arranged in the roof to discharge water and reduce the roof's water content, optimizing the engineering environment of the roadway in mudstone weakly cemented surrounding rock. The surrounding rock properties are improved through grouting, sealing the roof seepage channels, and using reasonable bolts (or anchor cables) for active support to reinforce the anchoring-bearing structure. This controls the deformation of the return airway in the 1801 working face of the Danan Lake No. 5 Mine, achieving stable control of the mudstone weakly cemented surrounding rock.

The parameters for the bolt and cable support in the return air lane of the 1801 fully mechanized working face are as follows:

Roof: Φ22×L2400mm left-hand threaded steel bolts without longitudinal

ribs, with a spacing of 800×800mm. Each bolt is anchored using 1 MSK2335 and 1 MSZ2350 resin anchor, equipped with a 150mm × 150mm × 10mm butterfly plate. Reinforcement cables use Φ18.9 × L6300mm high-strength anchor cables, arranged in a '3-2-3' pattern, with a row spacing of 1600mm. Each row has three cables spaced 2000mm apart, and two cables spaced 2400mm apart. Each cable is anchored using 2 MSCK2335 and 2 MSZ2350 resin anchors, equipped with a 300mm×300mm×16mm butterfly plate. Both bolts and cables are connected with ladder beams made of Φ14mm round steel and assisted by a metal mesh made of #12 iron wire for surface support, with mesh openings of 50×50mm.

Support: Φ22×L2400mm left-handed deformed steel anchor rods without longitudinal ribs, spaced at 800×800mm, with anchoring agent and trays the same as those used for roof plate anchor support.

In order to understand the deformation and failure conditions of mudstone weakly cemented roadway surrounding rock, as well as the stress conditions and stability of the bolt (anchor) support structure, and further evaluate the support effect to ensure the stability of mudstone weakly cemented roadway under hydrodynamic action, a comprehensive monitoring station was set up in the newly excavated section of the return air roadway at the 1801 working face, as shown in Fig.19. The specific monitoring content includes delamination of the roadway roof, displacement changes on the roadway surface, and the stress state of the bolts (anchors), with the main observation equipment shown in Fig.20.

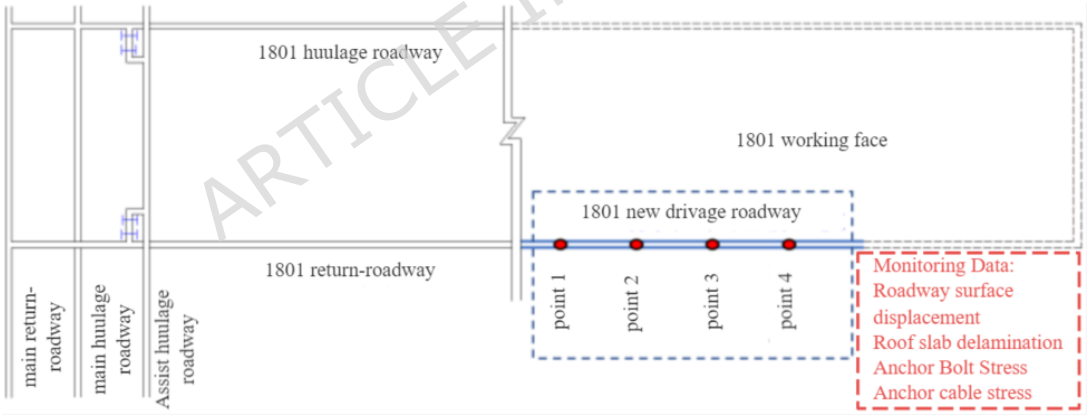

Figure 19 Comprehensive station layout of the new excavation section of the tailgate of the 1801 working face of the No. 5 mine in Dananhu

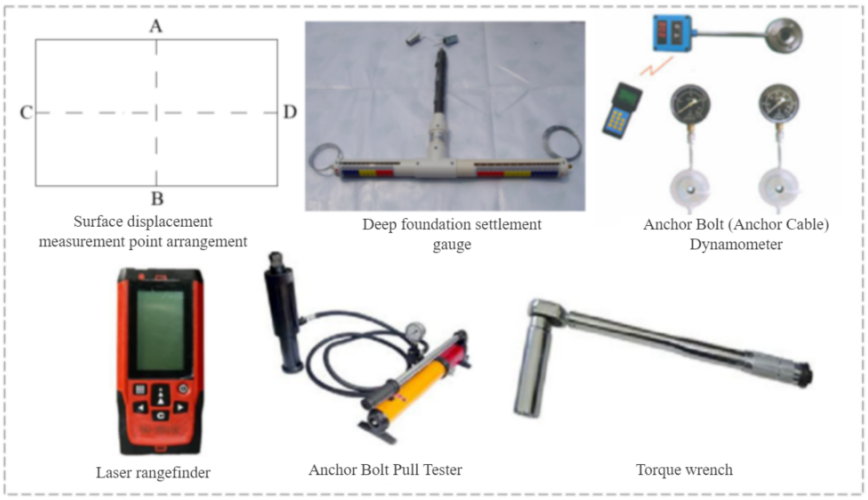

Figure 20 Mine pressure observation equipment in the tailgate of the 1801 working face of the No.5 mine Dananhu

4.4 Test results

（1）Deformation Amount of Return Air Roadway at 1801 Working Face

Based on observations of the deformation in the newly excavated section of the return airway of the 1801 working face, as the distance between the comprehensive survey station and the advancing working face increases, the deformation rate of the surrounding rock in the return airway of the 1801 working face gradually slows down and eventually stabilizes. When approximately 200 meters behind the excavation face, the roof settlement of the roadway reaches a maximum of about 140 mm and stabilizes, and when about 110 meters from the excavation face, the maximum convergence of the two sides reaches approximately 84 mm and stabilizes. This verifies the effectiveness of the proposed control technology and parameters, demonstrating that it can control the deformation of roadways in weakly cemented muddy surrounding rock and achieve stability in such surrounding rock.

（2）Displacement of the deep benchmark on the return airway roof at working face 1801

Based on the observation of the deep benchmark displacement of the roof of the newly excavated section of the return airway in the 1801 working face, as the distance between the comprehensive survey station and the advancing working face increases, the displacement of each benchmark on the roof of the return airway of the 1801 working face first increases rapidly and then gradually stabilizes; the maximum detachment measured between the benchmarks at 3.5m, 4.5m, and 5.5m from the roadway roof is about 25mm. The maximum detachment measured between the benchmarks at 0.5m, 1.5m, and 2.5m from the roadway roof is about 30mm, indicating that the combined support of anchor bolts (anchor cables) and grouting can effectively control the deformation of the surrounding rock in the return airway of the 1801 working face.

（3）Axial load of bolts in the return air roadway of the 1801 working face

Based on the observation of the axial loads of the roof and side bolts in the newly excavated section of the return airway of working face 1801, as the distance from the comprehensive measuring station to the advancing working face increases, the axial loads of the roof and side bolts in the return airway of working face 1801 first increase and then tend to stabilize. When the distance is approximately 150 meters behind the heading of the advancing working face, the loads of the roof bolts and side bolts reach stable values. The axial loads of roof bolt 1, roof bolt 2, and the side bolt are 90 kN, 120 kN, and 60 kN, respectively. Their stable loads are all less than the breaking loads of the bolts; therefore, the bolt support components in the return airway of working face 1801 are in a stable state.

（4）Axial Load Monitoring of Anchor Cables in the Newly Excavated Section of the Return Air Roadway at Working Face 1801

Based on the observations of axial loads on roof bolts in the newly excavated section of the return airway of working face 1801, as the distance between the total station and the tunneling working face increases, the axial loads of the roof bolts in the return airway of working face 1801 first increase and then tend to stabilize. Within approximately 0–45 meters behind the tunnel face of the working face, the bolt loads increase significantly. About 110 meters behind the tunnel face, the bolt loads tend to stabilize, with axial loads of Roof Bolt 1, Roof Bolt 2, and Roof Bolt 3 being 155 kN, 190 kN, and 250 kN, respectively. Their stable loads are all less than the breaking loads of the bolts, ensuring the stability of the roadway.

5 Conclusion

In order to solve the problem of large deformation of surrounding rock in muddy weakly cemented roadway, the stability mechanism and control technology of this type of surrounding rock roadway are systematically studied. Through the combination of laboratory tests, numerical simulations, theoretical analysis and field tests, the disintegration characteristics of argillaceous weakly cemented rocks under hydraulic action are revealed, the constitutive model of argillaceous weakly cemented rocks considering the influence of hydraulics is established, the deformation and failure mechanism of this type of surrounding rock roadway is clarified, and the joint support technology of high-strength anchor (cable) is proposed. The research results were applied and verified in the No. 5 mine of Dananhu Lake. The main conclusions are as follows:

(1) A constitutive model of argillaceous weakly cemented rock considering cohesion c, internal friction angle φ and shear angle ψ evolution with equivalent plastic strain e^{ps} was established, and the whole process of rock stress-strain response in triaxial compression test was completely reproduced. The applicability of the model in simulating the expansion and large deformation behavior of argillaceous weakly cemented rocks is verified

by comparing numerical simulations with laboratory tests.

(2) Based on numerical simulations, the stress distribution characteristics of the surrounding rock of the roadway under different moisture content conditions and its evolution law over time are systematically analyzed. The results show that with the increase of moisture content, the stress concentration area of the surrounding rock gradually shifts to the depth, and the extreme value of the principal stress difference increases significantly, resulting in the aggravation of the risk of roadway deformation and instability, and the proximity of the top and bottom slab in the middle of the roadway also shows an increasing trend.

(3) The strengthening mechanism of high-strength bolt (cable) support on the formation of the surrounding rock bearing structure of the roadway is revealed, and the reasonable support parameters are determined. The numerical simulation results show that compared with the traditional support method, the roof subsidence, the amount of two gangs of approach, the amount of foot drum and the range of roof damage area of the muddy weakly cemented surrounding rock roadway are reduced by 35%, 26.1%, 50% and 35.7%, respectively, which significantly inhibits the deformation and failure development of the roadway.

Author Contributions

Yu Zaijiang is mainly responsible for the overall planning of the paper and the writing of the manuscript, Zhang Weiguang is mainly responsible for theoretical derivation and verification, Lun Zhi, Wang Rui, and Wang Shuai are mainly responsible for the numerical simulation aspects, and Zhao Leilei, Liu shuaigang is mainly responsible for on-site testing.

Funding and Acknowledgments

This research was funded by theXinjiang Tianshan Talent Training Program for Young Top-notch Talents (Research on the mechanism of disaster formation in weakly cemented roadway surrounding rock and the coordinated control technology of grouting modification-2024TSYCCX0051); Key Research and Development Special Tasks of Xinjiang Province (No.2022B01051-3).; Opening Foundation of Key Laboratory of Xinjiang Coal Resources Green Mining (Xinjiang Institute of Engineering), Ministry of Education (KLXGY-KB2509).; Doctoral Startup Fund of Xinjiang Institute of Engineering (2025XGYBQJ56); Xinjiang Uygur Autonomous Region Tianchi Elite Talent Innovation Leadership Program: 2024XGYTCYC03; Urumqi City Hongshan Sci-Tech Innovation Elite Talents Youth Top Talents Program: B241013004; National Key Research and Development Program Young Scientists Project: 2024YFC2910600; Internal Project of Key Laboratory of Xinjiang Coal Resources GreenMining, Ministry of Education: KLXGY-Z2603.

Data Availability

Data available on request from the corresponding author, Yu Zaijiang (yyzaijiang@126.com) due to restrictions.

Conflicts of Interest

The authors declare no conflict of interest.

References:

[1] Liu Honglin. Research on the Mechanism and Classification of Water-Conserving Mining in Extra-Thick Coal Seams of Weakly Cemented Strata in Ili [D]. Xuzhou: China University of Mining and Technology.2020.

[2] Zhao Z, Lv X, Wang W, et al. Damage evolution of bi-body model composed of weakly cemented soft rock and coal considering different interface effect[J]. SpringerPlus, 2016, 5(1): 292.

[3] Zhao Wei, Yu Fenghai, Zhao Tongbin, et al. Study on the Prestress of Anchor Cables in Weakly Cemented Soft Rock Roadways [J]. Mining Research and Development, 2020,40(02):109-113.

[4] Ji Hongguang, Chen Bo, Sun Lihui, et al. Study on Acoustic Emission Characteristics of Weakly Cemented Sandstone in Hongqinghe Coal Mine under Uniaxial Loading Conditions [J]. Metal Mines,2015(10):56-61.

[5] Ji Hongguang, Jiang Hua, Song Chaoyang, et al. Microscopic Structural Evolution and Fracture Morphology Analysis of Weakly Cemented Sandstone Softening when Exposed to Water [J]. Journal of Coal Science,2018,43(04):993-999.

[6] Song Chaoyang. Study on Microscopic Structural Characteristics and Deformation Failure Mechanisms of Weakly Cemented Sandstone and Its Applications [D]. Beijing: University of Science and Technology Beijing,2017.

[7] Song Chaoyang, Ding Zhenyu, Tan Jie, et al. Experimental study on acoustic emission characteristics of weakly cemented sandstone under cyclic disturbance stress [J]. Well Drilling Technology, 2019,40(04):26-30.

[8] Song Chaoyang, Ji Hongguang, Jiang Hua, et al. Acoustic Emission Characteristics of Weakly Cemented Sandstone under Wet-Dry Cycles and Its Microscopic Deterioration Mechanism [J]. Journal of China Coal Society,2018,43(S1):102-109.

[9] Song Chaoyang, Ji Hongguang, Liu Yangjun, et al. Factors Affecting the Disturbance of Adjacent Roadway Excavation under Weakly Cemented Surrounding Rock Conditions [J]. Journal of Mining and Safety Engineering,2016,33(05):806-812.

[10] Song Chaoyang, Ji Hongguang, Liu Zhiqiang, et al. Morphological characteristics and failure mechanism of shear fracture surfaces in saturated weakly cemented sandstone [J]. Journal of China Coal Society,2018,43(09):2444-2451.

[11] Song Chaoyang, Ji Hongguang, Liu Zhiqiang, et al. Experimental Study on Acoustic Emission Characteristics of Weakly Cemented Rocks under Wet-Dry Cycles [J]. Journal of Mining and Safety Engineering,2019,36(04):812-819.

[12] Song Chaoyang, Ji Hongguang, Zhang Yuezheng, et al. Influence of Principal Stress on the Stability of Weakly Cemented Soft Rock in

Matoumen Surrounding Rock [J]. Journal of Mining and Safety Engineering.2016,33(06):965-971.

[13] Song Chaoyang, Ning Fangbo. Research progress on the correlation between microstructural parameters of weakly cemented rocks and their macroscopic mechanical behavior [J]. Metal Mines,2018,520(12):7-15.

[14] Sun Lihui, Ji Hongguang, Yang Bensheng. Physical and mechanical properties of weakly cemented strata rocks in typical western mining areas [J]. Journal of Coal Science,2019,44(03):866-874.

[15] You S, Ji H, Wang T, et al. Thermal and mechanical coupling effects on permeability of weakly cemented sandstone[J]. Emerging Materials Research, 2018, 7(2): 100-108.

[16] Yao B, Shan R L, Ju Y et al. Study on the mechanical properties and damage constitutive model of frozen weakly cemented red sandstone[J]. Cold Regions Science and Technology, 2020, 171(C): 1-17.

[17] Yang Qi. Research on the Creep Mechanical Properties of Sandstone Mudstone in the Artificially Frozen Strata of the Western Cretaceous [D]. Xi'an: Xi'an University of Science and Technology.2018.

[18] Jiabing Zhang, Ronghuan Du, et al. The deformation and failure characteristics of tunnels in layered rock with gentle dip angles after freeze–thaw cycles: Physical model tests and numerical investigation[J]. Tunnelling and Underground Space Technology,2024, 144

Volume 144,

[19] Zhang, J., Zhang, X., et al. A constitutive model of freeze-thaw damage to transversely isotropic rock masses and its preliminary application[J]. Computers and Geotechnics, 2022, 152

[20] Zhang, Jiabing & Chen, et al. Macroscopic and microscopic mechanical characteristics and crack propagation behavior of sandstone-like samples with single cracks under freeze-thaw cycles: Experimental and numerical simulation[J]. . Theoretical and Applied Fracture Mechanics, 2023, 129.

[21] Wang P, Feng T, Zhu Y J, et al. Experimental study on secondary bearing mechanism of weakly cemented broken rock mass[J]. Journal of Vibroengineering, 2019, 21(8): 2228-2240.

[22] Li Wei, Qiao Weiguo, Lin Dengge, et al. Numerical Simulation of Joint Support in Extremely Weakly Cemented Mudstone Large-Deformation Roadways [J]. Coal Mine Safety.2016,47(08):226-229.

[23] Wang Peng. Research on the Deformation Law and Control Technology of Weakly Cemented Surrounding Rock Eroded by Alkaline Water in the Seventh Mine of Danan Lake [D]. Xuzhou: China University of Mining and Technology.2021.

[24] Wang Yunbo, Jing Jidong, Zhang Dequan, et al. Control Technology and Application of Deformation and Failure in Weakly Cemented Soft Rock Roadways [J]. Coal Mine Mining.2014,19(02):53-57.

[25] Zhang Weiguang, Zheng Xiaodong, Bai Jianbiao, et al. Current Situation and Control Strategies of Roof Disasters in Weakly Cemented Roadways in

Xinjiang Mining Areas [J]. Coal Mine Safety. 2023,54(06):163-169.
[26] He Guangliang, Wang Weiming, Zhang Weishe, et al. Research on the Cross-Section Form and Support Optimization of Weakly Cemented Soft Rock Roadways [J]. Coal Engineering. 2017,49(01):38-41.
[27] Li Jun, Li Xuebin, Wang Lei. Research on the Support Scheme of Weakly Cemented Soft Rock Main Inclined Shaft [J]. Journal of North China University of Science and Technology.2015,12(03):54-59.
[28] Gao Guangyuan, Zhuo Lu, Li Wenyi, et al. Research on Surrounding Rock Control Technology for Weakly Cemented Extremely Soft Rock Roadways [J]. Coal Technology. 2016,35(01):46-48.
[29] Cai Jinlong. Research on the Deformation and Instability Mechanism of Weakly Cemented Soft Rock Tunnels in the Jurassic System and Its Application [D]. Huainan: Anhui University of Science and Technology.2020.
[30] Zhang Zhizhen, Teng Yeqi, Zhou Rui, et al. A nonlinear micromechanical damage-plastic coupled constitutive model for rocks and its numerical implementation [J]. Chinese Journal of Rock Mechanics and Engineering.2024,43(06):1425-1442.
[31] Wang Kai, Zuo Xiaohuan, Du Feng, et al. Macro-meso damage characteristics and energy-damage constitutive model of coal-rock composite structures under cyclic loading [J]. Journal of China Coal Society,2024,49(02):767-784.
[32] Chen Huiguan, Zhao Cheng, Zhang Rui, et al. Rock elasto-plastic damage incremental constitutive model considering the characteristics of gap compaction [J]. Chinese Journal of Rock Mechanics and Engineering,2023,42(12):3043-3055.
[33] Chen Siyu, Wang Qingcheng, Yang Liyun. Research Progress on Dynamic Constitutive Models of Rock-Like Materials [J]. Science and Technology Review,2022,40(08):115-126.
[34] Hu Xuelong, Li Keqing, Qu Shijie. Rock elastoplastic constitutive model based on unified strength theory and its numerical implementation [J]. Explosion and Impact,2019,39(08):130-138.
[35] Ma Qiufeng, Qin Yueping, Zhou Tianbai, et al. Research on the Mechanical Properties and Constitutive Model of Multi-Porous Rocks Under Unloading [J]. Rock and Soil Mechanics,2019,40(07):2673-2685.
[36] Cai W, Zhu H, Liang W, et al. A post-peak dilatancy model for soft rock and its application in deep tunnel excavation[J]. Journal of Rock Mechanics and Geotechnical Engineering, 2023, 15(3): 683-701.
[37] Azadi A, Momayez M. Review on Constitutive Model for Simulation of Weak Rock Mass[J]. Geotechnics, 2024, 4(3): 872-892.
[38] Yan Bingqian, Ren Fenhua, Cai Meifeng, et al. A Review on Rock Physical and Mechanical Properties and Constitutive Models under Multi-Field Coupling Effects of THMC[J]. Journal of Engineering Science,2020,42(11):1389-1399.

[39] Zhang Chuhan. On the Discrete-Contact-Fracture Analysis of Rock and Concrete [J]. Journal of Rock Mechanics and Engineering,2008,(02):217-235.